VI International Conference on Particle-based Methods – Fundamentals and Applications
PARTICLES 2019
E. Oñate, M. Bischoff, D.R.J. Owen, P. Wriggers & T. Zohdi (Eds)

VERIFICATION AND VALIDATION IN HIGHLY VISCOUS FLUID SIMULATION USING A FULLY IMPLICIT SPH METHOD

Daniel S. Morikawa[1], Mitsuteru Asai[1] and Masaharu Isshiki[2]

[1] Departament of Civil Engineering
Kyushu University
744 Motooka Nishi-ku, 819-0395 Fukuoka, Japan
e-mail: daniel@civil.doc.kyushu-u.ac.jp, web page:
https://kyushu-u.wixsite.com/structural-analysis

[2] Graduate School of Science and Engineering
Ehime University
3 Bunkyo-cho, 790-8577 Fukuoka, Japan

Key words: SPH, Implicit time integration, Non-Newtonian fluids, Ghost particles

Abstract. Catastrophes involving mass movements has always been a great threat to civilizations. We propse to simplify the behavior of the mass movement material as a highly viscous fluid, possibly non-Newtonian. In this context, this study describes the application of two improvements in highly viscous fluid simulations using the smoothed particle hydrodynamics (SPH) method: an implicit time integration scheme to overcome the problem of impractically small time-step restriction, and the introduction of air ghost particles to fix problems regarding the free-surface treatment. The application of a fully implicit time integration method implies an adaptation of the wall boundary condition, which is also covered in this study. Furthermore, the proposed wall boundary condition allows for different slip conditions, which is usually difficult to adopt in SPH. To solve a persistent problem on the SPH method of unstable pressure distributions, we adopted the incompressible SPH [1] as a basis for the implementation of these improvements, which guarantees stable and accurate pressure distribution. We conducted non-Newtonian pipe flow simulations to verify the method and a variety of dam break and wave generated by underwater landslide simulations for validation. Finally, we demonstrate the potential of this method with the highly viscous vertical jet flow over a horizontal plate test, which features a complex viscous coiling behavior.

1 INTRODUCTION

Landslide, debris flow, avalanche and dam collapse are examples of mass movement events. They are among the most harmful and widespread forms of disasters either natural or manmade. For instance, the 2019 tsunami in Indonesia, aka 2018 Sunda Strait tsunami, was caused by an underwater landslide triggered by Anak Krakatau volcano eruption. It

caused more than 400 deaths and 14 thousand injured people. Another example is the Brumadinho dam disaster in Brazil, 2019. The iron ore tailings dam collapse led to a mudflow that inundated a large area of the city of Brumadinho. More than 200 people lost their lives. Given the recent concern in this topic, it is essential for present and future public administrators to prepare preventive measures for mass movement events, which requires extensive studies on the phenomenon.

We propose to use the SPH method to simulate the bahavior of mass movements approximating its rheology into a non-Newtonian fluid, which can reach high viscosities. Here, we show a verification and validation (V & V) procedure of the method for different settings, which resulted in good agreement with theoretical solutions and past physical experiments.

2 SPH METHOD FORMULATION

The SPH method is one of the several Lagrangian mesh-free particle methods which was first proposed simultaneously by Lucy [2] and Gingold and Monaghan [3] in 1977 and it is widely applied to fluid dynamics problems. In this section, we present the basic aspects of this method.

2.1 Governing equations

The ISPH is designed to solve numerically the two main equations of hydrodynamic problems of incompressible flows, the continuity equation and the NavierStokes equation, respectively,

$$\nabla \cdot \mathbf{v} = 0, \tag{1}$$

$$\frac{D\mathbf{v}}{Dt} = -\frac{\nabla P}{\rho} + \nabla^2(\nu \mathbf{v}) + \mathbf{g}, \tag{2}$$

where $\mathbf{v}$ is the velocity vector, D/Dt the time derivative, P the pressure field, ρ the density of the fluid, ν the kinematic viscosity, $\mathbf{g}$ the external forces vector, and t the time.

2.2 SPH approximations

The SPH method is a space integration method that smoothly approximates the value of functions and its derivatives by integrating the contribution of the neighbor particles varying its influence according to a weight function W, which is chosen from a wide range of possibilities. In this study, we speted for the quintic spline function [4]. Then, one can approximate the value of a generic function ϕ for a given particle and its derivatives as

$$\langle \phi_i \rangle = \sum_{j=1}^{N} \frac{m_j}{\rho_j} \phi_j W(\mathbf{r}_{ij}, h), \tag{3}$$

$$\langle \nabla \phi_i \rangle = \frac{1}{\rho_i} \sum_{j=1}^{N} m_j (\phi_j - \phi_i) \nabla W(\mathbf{r}_{ij}, h), \tag{4}$$

$$\langle \nabla \phi_i \rangle = \rho_i \sum_{j=1}^{N} m_j \left(\frac{\phi_j}{\rho_j^2} + \frac{\phi_i}{\rho_i^2}\right) \nabla W(\mathbf{r}_{ij}, h), \tag{5}$$

$$\langle \nabla^2 \phi_i \rangle = \frac{2}{\rho_i} \sum_{j=1}^{N} m_j \frac{\mathbf{r}_{ij} \cdot \nabla W(\mathbf{r}_{ij}, h)}{\mathbf{r}_{ij}^2} (\phi_i - \phi_j), \tag{6}$$

where the subscripted indices i and j labels the target and neighboring particles, respectively, m is the mass, $\mathbf{r}_{ij} = \mathbf{x}_i - \mathbf{x}_j$ the relative position vector between particles i and j, and symbol $\langle\ \rangle$ signifies the application of the SPH approximation. Note that there are two formulations to approximate the first spatial derivative of a function as expressed by Eqs. 4 and 5.

3 FULLY IMPLICIT TIME INTEGRATION SCHEME

The original time integration scheme for the ISPH method [1] is based on a projection method which updates the velocity in a semi-implicit manner divided into two steps: predictor and corrector steps. In a similar way, we propose a fully-implicit time integration scheme using the same predictor and corrector steps [5]. The objective is to avoid the Courant-Friedichs-Lewy condition [6] on the maximum allowed time increment, which could lead to infeasibly small values for highly viscous fluid simulations.

3.1 Time integration based on the projection method

First, the contribution of the viscous term and the external forces of Eq.2 results in a predicted velocity field calculated implicitly as

$$\mathbf{v}^* = \mathbf{v}^n + \Delta t(\nabla^2(\nu \mathbf{v}^*) + \mathbf{g}). \tag{7}$$

Then, the pressure is calculated from a pressure Poisson equation

$$\nabla^2 P^{n+1} = \frac{\rho_0}{\Delta t} \nabla \cdot \mathbf{v}^* + \alpha \frac{\rho_0 - \rho^n}{\Delta t^2}. \tag{8}$$

Finally, adding the contribution of the pressure field, we calculate implicitly the updated velocity field as

$$\mathbf{v}^{n+1} = \mathbf{v}^* + \Delta t\Big(- \frac{\nabla P^{n+1}}{\rho_0}\Big). \tag{9}$$

In the above equations, Δt is the time increment, ρ_0 the reference density of the fluid, ρ_n a SPH approximation of the density based on Eq.3, α a relaxation coefficient, n and $n+1$ indices referring to the current and next iterations, and the superscript $*$ indicates the predictor step. Eqs. 7 and 9 are referred to as the predictor and corrector steps, respectively.

3.2 Rheological model

In this study, we use three different rheological models: Newtonian, Bingham plastic and Bingham pseudoplastic fluids.

In Newtonian fluids, the viscosity parameter has a fixed value, so $\nu = \nu_0$. In contrast, Bingham plastic and Bingham pseudoplastic rheologies are evaluated using the cross model and the Herschel-Bulkley model, respectively,

$$\tilde{\nu} = \nu_0 + \frac{\tau_y}{\dot{\gamma}\rho_0}, \tag{10}$$

$$\tilde{\nu} = \frac{K\dot{\gamma}^{n_0-1}}{\rho_0} + \frac{\tau_y}{\dot{\gamma}\rho_0}, \tag{11}$$

where $\tilde{\nu}$ represents the approximated viscosity, ν_0 the initial viscosity, K the consistency index, n_0 the flow behavior index, τ_y the yield stress, and $\dot{\gamma}$ the equivalent strain rate approximated as [7]

$$\dot{\gamma}_i^2 = \frac{1}{2}\sum_{j=1}^{N} m_j \frac{\rho_i + \rho_j}{\rho_i\rho_j} \frac{\mathbf{r}_{ij}\cdot\nabla W(\mathbf{r}_{ij},h)}{\mathbf{r}_{ij}^2} |\mathbf{v}_i - \mathbf{v}_j|^2. \tag{12}$$

To avoid numerical problems of dividing by zero, the final viscosity is evaluated as

$$\nu = \begin{cases} \nu_{MAX} & \text{if } \tilde{\nu} > \nu_{MAX} \\ \tilde{\nu} & \text{otherwise.} \end{cases} \tag{13}$$

3.3 Discretization of the governing equations

Using the SPH approximations of Eqs. 4, 5 and 6, we discretize Eqs. 7, 8 and 9 as

$$\mathbf{v}_i^* = \mathbf{v}_i^n + \Delta t\Big(\sum_{j=1}^{N} B_{ij}(\mathbf{v}_i^* - \mathbf{v}_j^*) + \mathbf{g}\Big), \tag{14}$$

$$\sum_{j=1}^{N} A_{ij}(P_i^{n+1} - P_j^{n+1}) = b_i, \tag{15}$$

$$\mathbf{v}_i^{n+1} = \mathbf{v}_i^* + \Delta t\Big(-\sum_{j=1}^{N} m_j\Big(\frac{P_j^{n+1}}{\rho_j^2} + \frac{P_i^{n+1}}{\rho_i^2}\Big)\nabla W(\mathbf{r}_{ij},h)\Big). \tag{16}$$

where

$$B_{ij} = m_j \frac{\rho_i\nu_i + \rho_j\nu_j}{\rho_i\rho_j} \frac{\mathbf{r}_{ij}\cdot\nabla W(\mathbf{r}_{ij},h)}{\mathbf{r}_{ij}^2}, \tag{17}$$

$$A_{ij} = \frac{2}{\rho_i} m_j \frac{\mathbf{r}_{ij}\cdot\nabla W(\mathbf{r}_{ij},h)}{\mathbf{r}_{ij}^2}, \tag{18}$$

$$b_i = \frac{1}{\Delta t}\sum_{j=1}^{N} m_j(\mathbf{v}_i - \mathbf{v}_j)\nabla W(\mathbf{r}_{ij},h) + \alpha\frac{\rho_0 - \rho_i^n}{\Delta t^2}. \tag{19}$$

Notice that Eq.17 uses a slightly different SPH discretization compared to Eq.6 to result in a symmetric linear equation. In addition, it was necessary to simplify the viscosity term on Eq.17 as the viscosity of the previous time step n, since the strain rate (Eq.12) is non-linear by nature.

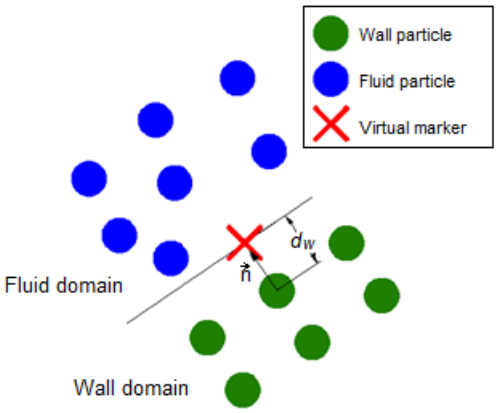

Figure 1: Wall boundary particles input information and virtual marker

4 BOUNDARY TREATMENT

For the correct application of the abovementioned equations, we need to define the boundary conditions accordingly. We propose the usage of ghost particles for both solid wall and free-surface boundaries.

4.1 Solid wall boundary

Following a similar procedure as [8], we selected a fixed wall ghost particle (FWGP) approach for the treatment of the solid wall boundary. First, fixed wall particles are placed in the wall domain, in which, for every wall particle, it is necessary to provide the normal direction $\mathbf{n}$ and the distance to the wall surface d_w as input information. Then, a virtual marker is placed on the boundary surface, as Fig.1 shows schematically.

To evaluate different slip conditions, we define the γ_{slip} parameter, which correspond to the percentage of slip on the projection of the velocity over the wall surface; that is, $\gamma_{slip} = 0$ means no-slip condition, $\gamma_{slip} = 0$, free-slip condition, and $1 > \gamma_{slip} > 0$, general slip condition.

Decomposing the velocity of a fluid particle(subscript f) near a wall particle (subscript w) into normal (subscript n) and orthogonal directions (subscript t) leads to

$$\mathbf{v}_{f,n} = (\mathbf{n}_w \cdot \mathbf{v}_f)\mathbf{n}_w, \tag{20}$$

$$\mathbf{v}_{f,t} = \mathbf{v}_f - \mathbf{v}_{f,n}. \tag{21}$$

where $\mathbf{n}_w$ represents the normal direction of a wall neighbouring particle.

Then, we derived the geometrical relationship

$$\mathbf{v}_{w,t} = C\mathbf{v}_{f,t}, \tag{22}$$

where

$$C = \gamma_{slip} - \frac{(1-\gamma_{slip})d_w}{|\mathbf{x}_f - \mathbf{x}_w|cos\theta - d_w}, \tag{23}$$

$$cos\theta = \frac{\mathbf{n}_w \cdot (\mathbf{x}_f - \mathbf{x}_w)}{|\mathbf{x}_f - \mathbf{x}_w|}. \tag{24}$$

Let's define the no-penetration condition as

$$\mathbf{v}_{w,n} = -\mathbf{v}_{f,n}. \tag{25}$$

Then, using Eqs. 22 and 25 leads to

$$\mathbf{v}_w = C\mathbf{v}_f - (1 + C)(\mathbf{n}_w \cdot \mathbf{v}_f)\mathbf{n}_w, \tag{26}$$

which can be interpreted as a relationship between the velocity of a target fluid particle and its wall neighbouring particle; therefore, can be applied on Eq.7.

Next, we define the pressure in the wall ghost particles based on a Neumann boundary condition stating that the acceleration $\mathbf{a}$ of the water particles close to the boundary surface in the normal direction of the wall should be zero; in other words,

$$\mathbf{a} \cdot \mathbf{n} = 0. \tag{27}$$

We then project the NavierStokes equation, Eq.2, along the normal to derive

$$\mathbf{a} \cdot \mathbf{n} = [-\frac{\nabla P}{\rho} + \nabla^2(\nu\mathbf{v}) + \mathbf{g}] \cdot \mathbf{n}, \tag{28}$$

$$\frac{\partial P}{\partial \mathbf{n}} = \rho(\nabla^2(\nu\mathbf{v}) + \mathbf{g}) \cdot \mathbf{n}, \tag{29}$$

$$P_w = P_{w,VM} - d_w\rho(\nabla^2(\nu\mathbf{v}) + \mathbf{g}) \cdot \mathbf{n}, \tag{30}$$

where the index VM represents the virtual marker of a wall particle.

Similarly to the velocity boundary condition, Eq. 30 can be applied to Eq.15 in the case of a target fluid i particle and its neighbouring wall particle j, since it is a general relationship between fluid and wall particles. However, to simplify this calculation, similarly to [8], we propose to approximate the pressure of a virtual marker J linked to the neighbouring wall particle j as

$$P_J^{n+1} = (1 - \beta)P_i^{n+1}. \tag{31}$$

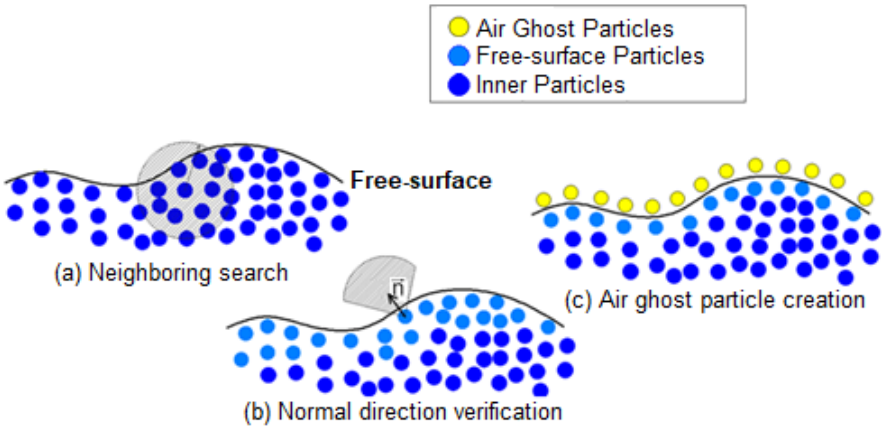

Figure 2: Process of creating AGPs

4.2 Free-surface boundary

In the original SPH method, there is no transition between inner fluid particles and void spaces outside the fluid domain, which causes some instability on the free-surface particles. Here, we propose the implementation of AGPs to create a fictitious mass around the free-surface to overcome this problem.

The algorithm described here is inspired by the space potential particle implementation [9] as follows. First, during the neighbouring search procedure, we attach the free-surface particle label for those with less than 160 neighboring particles in 3D simulations. Then, with an algorithm proposed by Marrone et al. [10], we reaffirm the free-surface particle label for those that have no particles in the conical plus a hemispherical region in the normal direction of each particle. Lastly, we create an AGP in the normal direction of each free-surface particle. Fig. 2 schematically illustrates this process.

If necessary, one may repeat processes (b) and (c) in Fig. 2 as often as needed to fill entirely the domain of influence of all free-surface particles. For the quintic spline weight function used in this study, three layers of AGPs are necessary to achieve the highest accuracy.

Null divergence of the velocity field on the free-surface particles boundary condition must be satisfied, which leads to a simplification in which the velocities of neighbouring AGPs are equal to the velocity of the fluid target particle. In addition, the zero pressure Dirichlet boundary condition must be satisfied on the AGPs.

5 NUMERICAL EXAMPLES

Here, we demonstrate the efficiency of the proposed SPH method with several numerical examples. The objective is to show a full process of verification and validation (V & V). First, the implicit time integration scheme is verified through several pipe flow simulations. Then, we validate it with dam break numerical tests, channel flow and underwater landslide. To finalize, we demonstrate the robustness of this method with the viscous coiling behavior.

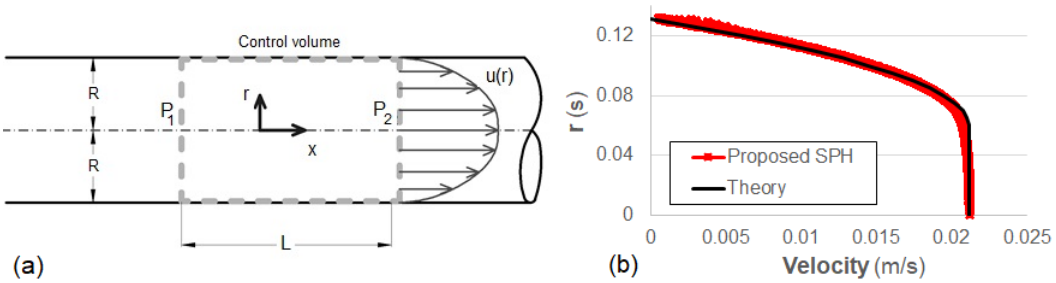

Figure 3: (a) Geometrical parameters of the pipe flow ; (b) Comparison between numerical and theoretical results of the non-Newtonian pipe flow simulation

5.1 Non-Newtonian pipe flow

We conducted the non-Newtonian pipe flow problem for the Bingham fluid, to verify our implicit time integration technique of the viscous term and the wall boundary treatment. Fig.3(a) illustrates the geometrical parameters of this problem. We utilized the following parameters during the simulation: R = 0.1325m, P1 = 2000Pa and P2 = 1000Pa (P = 1000Pa), L = 0.6m, 0 = 0.1m2/s, and d = 0.005m. Fig.3(b) is a graph comparing the numerical results with the theoretical solution. The theoretical value of the pipe flow velocity for Bingham plastic fluid is defined as [11]

$$u(r) = \begin{cases} \frac{\Delta P R^2}{4\rho\nu_0 L}\left[\left(1-\frac{2L\tau_y}{\Delta R}\right)^2\left(\frac{r}{R}-\frac{2L\tau_y}{\Delta R}\right)^2\right] & \text{if } r > r_0 \\ \frac{\Delta P R^2}{4\rho\nu_0 L}\left[\left(1-\frac{r_0}{R}\right)^2\right] & \text{if } r \leq r_0, \end{cases} \tag{32}$$

where

$$r_0 = \frac{2L\tau_y}{\Delta P}. \tag{33}$$

As expected, the numerical results are very consistent with the theoretical values.

5.2 Non-Newtonian Dam break

In this section, we conducted a series of dam break validation tests. First, we selected the well-known experimental study from Martin and Moyce [12] to verify the proposed SPH method applied on simple low viscosity case. To maintain the same notation as utilized in [12], lets define the non-dimensional quantities

$$T = t\left(\frac{g}{a}\right)^{1/2}, \tag{34}$$

$$Z = \frac{z}{a}, \tag{35}$$

where t is the time after the dam collapse, g is the gravity acceleration, a is the base length of the fluid, and z is the distance of the surge front from the initial wall. The chosen parameters in this validation test are $Height = a = 0.056m$, width $= 0.056m$, $d = 0.002m$, $\rho_0 = 1000kg/m^3$, $\nu_0 = 1.4 \cdot 10^{-7}m^2/s$, and $\Delta t = 1 \cdot 10^{-4}s$.

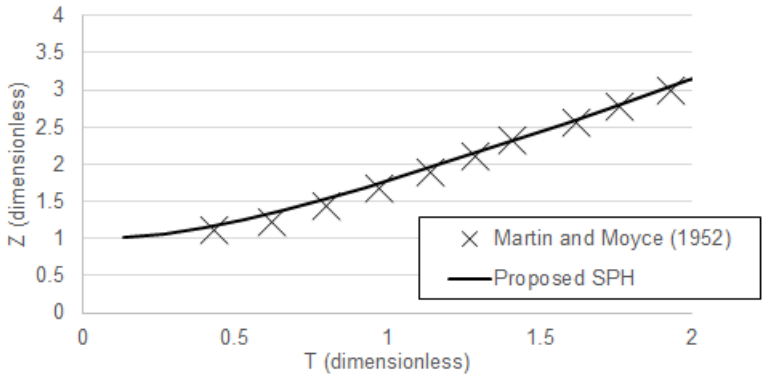

Figure 4: Comparison between numerical and experimental results of the Newtonian dam break simulation

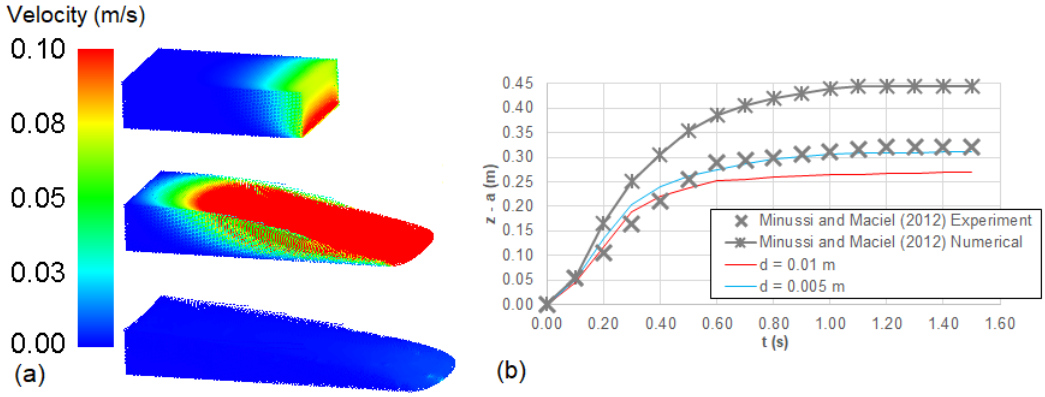

Figure 5: Non-Newtonian dam break: (a) Particle positioning after 0s, 1s and 1.5s of simulation; (b) Comparison of the non-Newtonian dam break results with [13]

Fig. 5.2 shows the simulation results graphically for the proposed SPH method. As expected, the results are very accurate.

Next, we analyze the dam break of a Bingham pseudoplastic fluid comparing with experimental results from Minussi and Maciel [13]. The following parameters were used in this verification test: height $= 0.13m$, $a = 0.5m$, width $= 0.32m$, $\rho_0 = 1000kg/m^3$, $\tau_y = 49.179Pa$, $k = 7.837Pa\,s^{n_0}$, $n_0 = 0.442$, $\nu_{MAX} = 100m^2/s$, and $\Delta t = 1 \cdot 10^{-4}s$.

Fig.5(a) shows the particle distribution of the non-Newtonian daybreak verification test after 0s, 1s and 1.5s of simulation, and Fig.5(b) shows the comparison between the results with different particle resolutions ($d = 0.01m$ and $d = 0.005m$). The results become more accurate as the particle resolution is finer, which shows the convergence of the proposed method. Also, as showed in Fig.5(b), our proposed method resulted in a better accuracy than the reference numerical solution presented in [13].

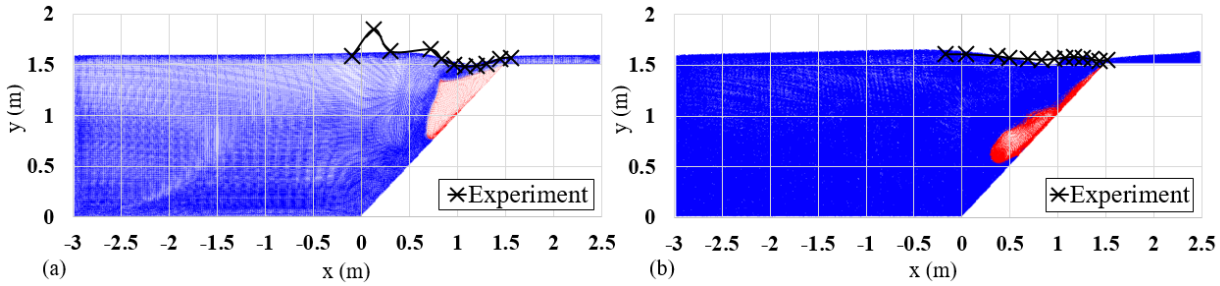

Figure 6: Underwater landslide comparison between the numerical solution and experiments from [16] at (a) 0.4s and (b) 0.8s

5.3 Underwater landslide

The next example is a validation test involving a multi-phase problem. [16] in collaboration with CEMAGREF institute (Centre National du Machinisme Agricole du Gnie Rural des Eaux et des Forts, France) conducted an experiment to evaluate the waves generated by underwater mass movements in a small scale experiment. The experiments consists of a portion of sand sliding over a frictionless plane inclined at 45 degrees. Initially, the channel with geometry specified in Fig.6 is filled with water at 1.6m depth and a sand mass of triangular cross section of 0.65m x 0.65m is positioned at the top of the inclined plane.

The numerical parameters are listed in table 1. As demonstrated in Fig.6, the numerical results are consistent with the experimental results, with the exception of one instance at 0.4s, which shows one data point that seems to not agree with the present numerical solution. We hypothesize that this one divergent data point might have been generated by the abrupt opening of the gate that was holding the sand mass at the initial position. In addition, this example shows the capability of our proposed method to simulate the no-slip condition at the inclined plane ($\gamma_{slip} = 0$).

Table 1: Parameters of the underwater landslide numerical test

d (m)	Δt (s)	$\rho_{0,water}$ (kg/m^3)	ν_{water} (m^2/s)	$\rho_{0,sand}$ (kg/m^3)	$\nu_{0,sand}$ (m^2/s)	$\tau_{y,sand}$ (Pa)
0.01	$1 \cdot 10^{-5}$	1000	$1.4 \cdot 10^{-7}$	1950	$5 \cdot 10^{-5}$	250

5.4 Viscous coiling

The viscous coiling behavior is a widely used benchmark test for highly viscous fluid simulation, since it is not possible to generate it without special treatment citeVileauRodgers. It is expected that viscous coiling behavior occurs on a vertical jet flow over a horizontal plate experiment, with a high enough viscosity and H/D (height over diameter) proportion [15].

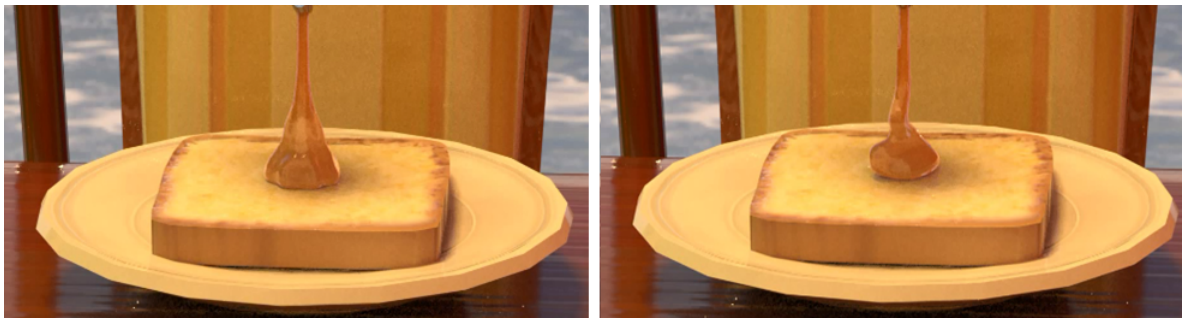

Figure 7: Vertical jet flow example without (left) and with (right) AGPs

The objective is to represent the behavior of honey falling over a bread. First, Fig.7 (left) reveals a rendered visualization of the vertical jet flow without the application of AGPs. Since the free-surface condition is not well verified, coiling could not occur, and the result is a radial motion. As oppose to that, Fig.7 (right) shows the same simulation solved with the introduction of AGPs. In this example, coiling occurs as a result of the improved free-surface treatment, and the movement appears to be very natural.

6 CONCLUSIONS

We proposed several improvements for highly viscous fluid and non-Newtonian fluid simulations using the SPH method. The main improvements are related to an implicit time integration scheme with a special boundary treatment of both the free-surface and the wall boundary using ghost particles. In addition, our proposed wall boundary approach (FWGP) may be applied to different slip conditions.

In the numerical tests, we validated our method using pipe flow numerical tests with non-Newtonian Bingham plastic rheology model. Next, we validated it with several dam break and underwater landslide simulations, which exhibited highly accurate results compared to previous experiments. Furthermore, we demonstrated the robustness of our improvements with a coiling behavior test of a highly viscous fluid. Although the free-surface treatment without AGPs in this last example could not reproduce the coiling behavior, our proposed model with FWGPs and AGPs naturally reproduces the coiling behavior.

As for future work, we plan to test the accuracy of this method in simulating large scale disasters such as landslides and debris flow. For this, we need to increase the computational speed and memory capacity of the program using high-performance computing (HPC) with expanding slice grid domain decomposition. In addition, we plan to couple this method with an SPH formulation for solid Mechanics to forecast the occurrence of landslides for different situations.

REFERENCES

[1] Asai, M., Aly, A.M., Sonoda, Y. and Sakai Y. A stabilized incompressible SPH method by relaxing the density invariance condition. *Int. J. Appl. Math.* (2012)

2012:139583. https://doi.org/10.1155/2012/139583.

[2] Lucy, L.B. A Numerical Approach to the Testing of the Fusion Process. *Astron. J.* (1977) **88**:1013-1024.

[3] Gingold R.A., Monaghan J.J. Smoothed Particle Hydrodynamics: Theory and Application to Non-Spherical Stars. *Astron. Soc.* (1977) **181**:375-389. https://doi.org/10.1155/2012/139583.

[4] Schechter H., Bridson R. Ghost SPH for Animating Water. *Proceedings of SIGGRAPH 2012 Conference 31* (2012) **4**, Article No. 61.

[5] Morikawa, D.S., Asai, M., Nur'Ain, I., Imoto, Y., Isshiki, M. Improvements in highly viscous fluid simulation using a fully implicit SPH method. *Comp. Part. Mech.* (2019) https://doi.org/10.1007/s40571-019-00231-6.

[6] Violeau D., Leroy A. On the maximum time step in weakly compressible SPH. *J. Comput. Phys.* (2014) **256**:388-415. <hal-00946833>.

[7] Violeau D., Issa R. Numerical modelling of complex turbulent free-surface flows with the SPH method: an overview. *Int. J. Numer. Meth. Fl.* (2007) **53**:277-304. <10.1002/d.1292><hal-01097824>.

[8] Idris, N.A., Sonoda, Y. A Multi-Scale Tsunami Simulations Based on 2D Finite Difference Method and 3D Particle Method with a Virtual Wave Maker. *Kyushu University Doctoral Dissertation* (2017).

[9] Tsuruta N., Khayyer A., Gotoh H. Space Potential Particles to Enhance the Stability of Projection-based Particle Methods. *Int. J. Numer. Meth. Fl.* (2015) DOI: 10.1080/10618562.2015.1006130.

[10] Marrone S., Colagrossi A., Le Touz D., Graziani G. Fast Free-surface Detection and Level-set Function Definition in SPH Solvers. *J. Comput. Phys.* (2010) **229**:3652-3663.

[11] Mattiusi E.M. Escoament Laminar de Fluid Newtonianos Generalizados em Tubos de Seo Transversal Elptica. *Doctoral Dissertation of the Federal Technological University of Paran* (2007).

[12] Martin J., Moyce W. An experimental study of the col-lapse of liquid columns on a rigid horizontal plane. *Philos. Trans. R. Soc. Lond.* (1952) **244**:312-324.

[13] Minussi R.B., Maciel G.F. Numerical experimental com-parison of dam break flows with non-Newtonian fluids. *J. of the Braz. Soc. of Mech. Sci. Eng.* (2012) **XXXIV**:2/167.

[14] Violeau D., Rogers B.D. Smoothed Particle Hydrodynamics (SPH) for Free Surface Flows: Past, Present and Future. *J. Hydraul. Res.* (2016) **54**:1-26.

[15] Tom M.F. et. al. A Numerical Method for Solving Three-dimensional Generalized Newtonian Free Surface Flows. *J. Nonnewton. Fluid Mech.* (2004) **123**:85-103.

[16] Rzadkiewicz, S.A., Mariotti, C. and Heinrich, P. Modelling of submarine landslides and generated water waves. *Phys. Chem. Earth* (2004) **123**:-2, pp.7-12 (1996).